J Sol-Gel Sci Technol (2014) 69:207–213
DOI 10.1007/s10971-013-3205-4

ORIGINAL PAPER

A new photoluminescent silica aerogel based on *N*-hydroxysuccinimide–Tb(III) complex

Corneliu Sergiu Stan · Nathalie Marcotte · Marius Sebastian Secula · Marcel Popa

Received: 3 July 2013 / Accepted: 3 November 2013 / Published online: 12 November 2013

Abstract The paper describes the preparation of a new photoluminescent silica aerogel by embedding a new Tb(III) complex in a silica matrix by using N-hydroxysuccinimide as ligand. The Tb(III) complex prepared at a metal to ligand ratio of 1:3 (mol%) exhibits strong photoluminescence as a result of specific radiative transitions within the Tb(III) cation with the most intense peak located at 543 nm due to $^5D_4 \rightarrow {}^7F_5$ transition. The synthesized complex was doped in the silica matrix through a catalyzed sol–gel process. After ageing in ethanol, the alcogel was dried under supercritical regime by exchanging the ethanol with liquid carbon dioxide followed by supercritical evaporation. The leaching of the free complex from the alcogel during ageing and solvent exchange phases was found to be minimal most likely due to the interactions between chemical groups of complex with those specific to silica matrix. The obtained regular shaped monolithic aerogel preserved the remarkable photoluminescent properties and also improved the thermal stability of the free complex. Both, the free complex and doped aerogel were characterized through thermal analysis, FT-IR, powder X-ray diffraction, Scanning electron microscopy and fluorescence spectroscopy. For comparison purposes, an undoped silica aerogel was also prepared and investigated through FT-IR, BET analysis and powder X-ray diffraction. The excellent photoluminescent properties might recommend the prepared aerogel for applications in optoelectronic devices where photonic conversion materials are required.

Keywords Sol–gel method · Functional composite · Photoluminescent Tb(III) complexes · Aerogel · Luminescence

1 Introduction

The synthesis of new aerogels with photoluminescent compounds embedded in their structure opens a number of interesting perspectives for applications in various fields, and especially in optoelectronic devices, which can benefit from their specific features, such as very low density, low refractive indices and exceptional thermal stability [1, 2]. Another remarkable advantage consists in the possibility to shape the aerogel according to the application requirements. Moreover, since the preparation process does not need elevated temperatures, it is possible to embed in aerogel matrix even sensitive organic compounds.

Introducing various luminescent materials in silica matrix during the early stages of preparation is not a straightforward task since these additions may interfere with the sol–gel processes that might affect the overall properties of the aerogel, especially the consistency or mechanical strength. Another potential drawback is represented by the possible leaching of guest material from the silica matrix into the solvent medium during the solvent exchange processes commonly involved in aerogel preparation. Leaching could be limited or avoided by physical or chemical binding the guest material to the gel framework [3].

C. S. Stan (✉) · M. S. Secula · M. Popa
Faculty of Chemical Engineering and Environmental Protection, Gheorghe Asachi Technical University of Iasi, Prof. Dr. Docent Dimitrie Mangeron No. 73, 700050 Iasi, Romania
e-mail: stancs@tuiasi.ro

N. Marcotte
Institut Charles Gerhardt MACS, Ecole Nationale Supérieure de Chimie de Montpellier, 8 rue de l' Ecole Normale, 34296 Montpellier Cedex, France

In an earlier study [4], Glauser and Lee successfully prepared fluorescein and rhodamine 6G doped silica aerogels aimed for flat panel displays applications. Several recent approaches have led to the obtaining of fluorescent aerogels by embedding ZnO nanocrystals during the sol–gel process involved by the silica matrix preparation [5] or through hydrofluoric acid catalyzed reaction between silyl functionalized benzazole pigments and poly-et-oxysiloxane groups in a 2-propanol medium [6]. Photo-luminescent aerogels were also prepared by embedding CdSe-ZnS core–shell quantum dots in the silica matrix [7]. Various studies on the luminescence of lanthanide doped silicate sol–gel glasses using TMOS or tetraethyl orthosilicate (TEOS) as silica precursors were reported. Earlier studies used various Ln(III) salts embedded in silica matrix, while more recent studies reported the use of various lanthanide complexes in order to maximize the overall luminescence efficiency based on the antenna effect induced by the surrounding ligands [8]. Though, there are many studies concerning lanthanide complexes embedded in silica matrices leading to luminescent silica xerogels [9–11], photoluminescent aerogels based on lanthanide complexes are not such widely reported. This situation is due to the significant difference between the preparation paths of the silica xerogels containing lanthanide complexes and those required for obtaining a luminescent silica aerogel. Thus, in most cases, the preparation of xerogels doesn't involve solvent exchange stages (commonly required by the supercritical drying in case of aerogel preparation), which may wash out significant amounts of the trapped complex.

In the present work, a Tb(III)–NHSI complex was prepared and studied prior to embedment in the silica matrix. An aqueous solution of the prepared complex was added during the sol–gel preparation of the silica matrix, which was further processed for obtaining the aimed aerogel. It is shown that the novel prepared aerogel retains the photo-luminescent properties of the Tb(III)–NHSI complex. The leaching of free complex in the solvent mediums used in various stages of the process was found to be insignificant due to the interactions with the silica matrix as it will be further detailed.

2 Experimental procedure

2.1 Materials

N-Hydroxysuccinimide (NHSI) (97 %) and TEOS (>99.0 %) were purchased from Sigma-Aldrich. Terbium chloride ($TbCl_3 \times 6H_2O$, 99.9 %) was purchased from Alfa–Aesar. Ammonium hydroxide (28 %) and sodium fluoride (99.99 %) were provided by Merck Chemicals. Absolute ethanol and high purity Milli-Q water were used for preparation and washing operations.

2.2 Preparation of photo luminescent silica aerogel

A sample of $[TbL_3(H_2O)_3]$ complex is prepared for investigation purposes. First, aqueous solutions of terbium chloride and bidentate NHSI ligand were prepared in 1:3 (mol%) metal to ligand ratio. Terbium chloride solution was prepared by dissolving 1 mmol of $TbCl_3 \times 6H_2O$ in 1 mL high purity water. The ligand solution was prepared by dissolving 3 mmol of NHSI (denoted as HL) in 2 mL high purity water. The complex was obtained by mixing the prepared solutions. The complexation reaction was carried out at 40–45 °C under moderate stirring for about 90 min. After initial drying in ambient conditions, the complex was washed with Milli-Q water. The crystalline form of complex was obtained by removing water through evaporation at room temperature and further drying at 60–70 °C, under vacuum, till constant weight. In depth information on the preparation of the complex and structural investigations are described in our prior work [12].

For the intended photoluminescent aerogel preparation, a similar procedure was used to prepare the $[TbL_3(H_2O)_3]$ complex. However, the complex was kept in its aqueous solution prior to embedment. The silica matrix was prepared using TEOS as precursor under alkaline catalytic conditions according to the method described by Soleimani and Abbasi [13]. Thus, 2 mL TEOS and 4 mL Et-OH were added in a 15 mL plastic vial. The vial must allow an easy removal, given the fragility of the gel prior to supercritical drying. In the meantime, the catalyst solution was prepared by dissolving 0.4 g NaF and 5 mL $NH_3{*}H_2O$ stock solution in 20 mL Milli-Q water. The catalyst solution was kept in a sealed glass recipient. The entire quantity of the previously prepared aqueous complex solution was added into the reaction vial, which had briefly been shaken. Immediately, 0.15 mL of the catalyst solution is added into the reaction vial. During the gelation process, which usually takes about 90–120 min, the reaction vial had to be kept in a vibration free environment. After the gelation process ended, the gel was carefully transferred from the reaction vial in a 50 mL glass beaker which contains a volume of Et-OH that allows the gel to be completely immersed. Then, the gel was aged in Et-OH for at least 48 h [14]. The next stage involved further exchange of the remaining water in the gel structure by removing the ageing solution which is replaced with absolute ethanol. This operation was performed twice with at least 24 h between ethanol exchanges. In order to investigate the amount of free complex leached during ageing and solvent exchange operations, the entire quantity of Et-OH involved in these processes was collected in a glass recipient previously

weighed. After the Et-OH is removed through evaporation and further drying for about 24 h under vacuum at 40–45 °C the recipient was weighed again. After the drying procedure, an additionally 64 mg of solid compound deposited within the recipient was found. This represents approx. 12 % of the initial $[TbL_3(H_2O)_3]$ complex according to the quantities used in the described experiment. The obtained alcogel was finally dried in a pressure vessel by exchanging the ethanol with liquid CO_2 followed by supercritical evaporation, according to the method described by Pierre and Pajonk [15]. In our work, the process was carried out with a SPY-DRY critical point dryer setup. The method described has allowed obtaining a regular shaped aerogel with excellent photoluminescent properties due to the embedded $[TbL_3(H_2O)_3]$ complex.

2.3 Characterization techniques

The IR spectra were recorded in the range of 400–4,000 cm^{-1}, using a Bruker Vector 22 spectrometer, according to KBr pellet method. The thermal stability was studied using a Mettler Toledo TGA-SDTA851e, working in nitrogen atmosphere with a flow rate of 20 mL min^{-1}. The heating rate was adjusted to 10 °C min^{-1} in the range of 50–1,000 °C. The thermal decomposition parameters were provided by the accompanying software based on Freeman-Carroll method. The XRD patterns were recorded in the 5–70° 2θ range by means of a Panalytical X'Pert Pro diffractometer provided with a Cu-Kα radiation source (λ = 0.15406 nm). Unit cell parameters of the free complex were further refined using Panalytical X'Pert High Score Plus software. Scanning electron microscopy (SEM) micrographs were recorded with a Hitachi SU-1510 equipment, working at 15 kV accelerating voltage. The fluorescence emission and excitation spectra were recorded by means of an ISS-K2 fluorometer provided with a powder analysis adapter. The BET analysis was performed based on nitrogen adsorption–desorption isotherms obtained with Micromeritics ASAP 2020 equipment. Prior to investigation, the sample was degassed at 150 °C under vacuum.

3 Results and discussion

Either in aqueous solution for further embedding in silica matrix or in solid, crystalline state for characterization purposes, the synthesis of complexes involves the following chemical reaction between precursors:

$$TbCl_3 + 3C_4H_5NO_3 \rightarrow Tb(C_4H_4NO_3)_3 + 3HCl$$

Investigations reported in our previous work [12] revealed the following generic structure of the complex: $[TbL_3(H_2O)_3]$.

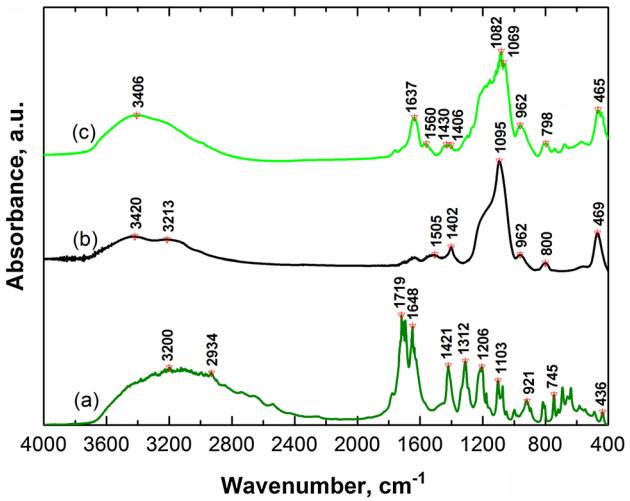

Fig. 1 Recorded FT-IR spectra for: **a** free $[TbL_3(H_2O)_3]$ complex, **b** undoped aerogel and **c** aerogel with embedded complex

Briefly, data provided by the chemical analysis, EDX and thermal analysis support the 1:3 combination ratio between Tb(III) cation and bidentate NHSI ligand and also the presence of three water molecules in the first coordination sphere. The coordination number achieved by the Tb^{3+} cation is 9. This is due to the participation of three ligand molecules with their bidentate behavior and three water molecules. The results are in agreement with other studies that indicate the same coordination number and the presence of three water molecules in complexes of trivalent lanthanide cations prepared with other bidentate ligands [16, 17].

3.1 FT-IR analysis

Data provided by the recorded FT-IR spectrum in case of the free $[TbL_3(H_2O)_3]$ complex (Fig. 1, line (a)) confirmed the characteristic absorption peak at 436 cm^{-1} of the established Ln–O–N < bond that occurs by replacing the hydrogen atom in the original H–O–N < groups in ligand. The coordinative bond between trivalent lanthanide cation and oxygen in carbonyl groups was highlighted by the shifting of the characteristic peaks of these bonds towards lower wave numbers due to the stretching of O=C < bonds. Present in the free ligand, the carbonyl specific peak occurs in case of the prepared complex split in two distinct peaks due to the participation at the coordinative bond of a single carbonyl group among the two groups existing in the free ligand. More details regarding the FT-IR analysis of the free ligand and the changes occurred through complexation are described in our previous work [12]. In order to investigate the changes arising from the embedment of $[TbL_3(H_2O)_3]$ complex in the aerogel structure, FT-IR absorption spectra were recorded for the prepared photoluminescent aerogel (Fig. 1, line (c))

and also for a sample of undoped aerogel prepared under similar conditions (Fig. 1, line(b)). For the undoped aerogel, the maximum intensity peak located at 1,095 cm^{-1} is attributed to the asymmetric stretching vibration of Si–O–Si bonds; the peak at 962 cm^{-1} is specific to the stretching vibrations of Si–O bonds, and the peaks located at 800 and 469 cm^{-1} are due to the symmetric stretching vibrations of Si–O–Si group and to the deformation vibration of O–Si–O bonds, respectively [18]. The wide peak located at 3,406 cm^{-1} (Fig. 1, line (c)) can be attributed to the stretching vibrations specific to water molecules retained in the structure of doped aerogel and can also be associated with hydrogen bonds occurring between –Si–OH…O–Si– and –Si–OH groups.

The spectrum recorded for the doped aerogel (Fig. 1, line (c)) shows significant changes compared to the undoped one (Fig. 1, line (b)). The new peaks occurring at 1,637/1,560 cm^{-1}, which cannot be seen in the undoped aerogel, are due to C=O carbonyl groups of the embedded complex (Fig. 1, line (a)). In the case of doped aerogel, these peaks are shifted to lower values (from 1,719/1,648 cm^{-1} in the free complex to 1,637/1,560 cm^{-1}, respectively in the doped aerogel) most probable due to the interactions occurring between these groups and silica matrix. Also, due to the disturbances occurring in the silica matrix through complex embedding, the maximum intensity peak initially located at 1,095 cm^{-1} in the undoped aerogel (Fig. 1, line (b)), which is specific to asymmetric stretching vibrations of the Si–O–Si bonds, is slightly displaced to 1,082 cm^{-1} in case of $[TbL_3(H_2O)_3]$ doped aerogel (Fig. 1, line (c)). These modifications are in agreement with the observations taken from SEM analysis (See the Sect. 3.5) and might explain the low leaching of the complex during the solvent exchange operations requested by the aerogel preparation. Low intensity 800 cm^{-1} peak due to Si–O–Si symmetric stretching vibrations recorded in the undoped aerogel spectrum (Fig. 1, line (b)) appears practically unaffected (798 cm^{-1}) in the doped aerogel spectrum (Fig. 1, line (c)). Also, the Tb–O bond vibration located at 436 cm^{-1} observed in case of the free complex is masked by the wider medium intensity 465 cm^{-1} peak specific to the deformation vibration of O–Si–O bond in silica matrix.

3.2 Powder X-ray diffraction

Figure 2 presents the recorded diffractograms of the photoluminescent aerogel and undoped aerogel samples. The recorded diffractograms show a typical silica amorphous structure, similar results being also reported in other studies [19]. As can be noted, the two recorded diffractograms are virtually identical due to the minimal influence induced by the small amount of complex in the aerogel volume and also by the interactions between functional groups of the

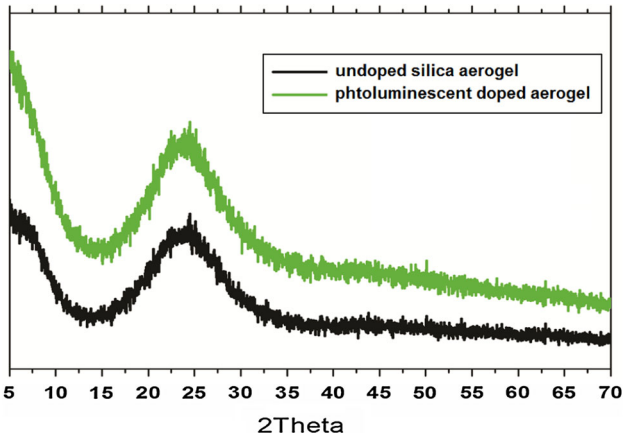

Fig. 2 Recorded diffractograms of undoped and photoluminescent doped aerogels

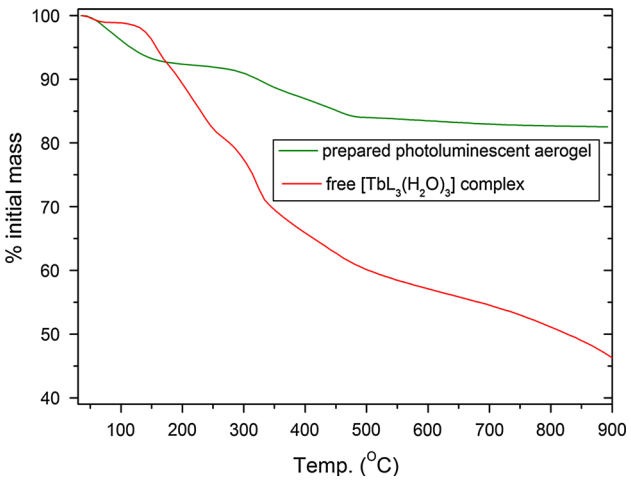

Fig. 3 Recorded thermal behavior for the free $[TbL_3(H_2O)_3]$ and aerogel with embedded complex

$[TbL_3(H_2O)_3]$ complex and those of silica matrix. Yet, the photoluminescence of the prepared aerogel indicates the presence of the $[TbL_3(H_2O)_3]$ complex attached to the silica matrix, the requirements for energy transfer towards the central Tb^{3+} cation being still fulfilled.

The P-XRD investigation of the free $[TbL_3(H_2O)_3]$ complex revealed its crystalline form with a monoclinic geometry. Further details regarding calculated unit cell parameters can be found in our previous work [12].

3.3 Thermal analysis

Figure 3 shows the mass loss recorded for the photoluminescent aerogel containing $[TbL_3(H_2O)_3]$ complex. For comparison purposes it is also presented the mass loss recorded for the free complex. In this case, the decomposition process of the free complex takes place in five stages

Table 1 Doped aerogel thermal behavior and decomposition parameters

Decomposition stage	Parameter	Doped aerogel
Stage 1	Pre-exponential factor	2.7×10^{16}
	Activation energy (kJ/mol)	22.89
	Reaction order	0.55
	Temp. interval (° C)	51–157
	% loss	7.82
Stage 2	Pre-exponential factor	1.24×10^{18}
	Activation energy (kJ/mol)	74.62
	Reaction order	0.49
	Temp. interval (° C)	272–580
	% loss	9.63
Residue %		82.53

[12], while in case of doped aerogel the process presents only two stages (Table 1) in the same range of temperature. Total mass loss recorded for the doped aerogel is about 17 %, while in case of the free complex is of more than 45 %.

In the first stage of doped aerogel decomposition, the 7.82 % mass loss occurring in the range of 50–160 °C is attributed to the elimination of residual water retained in aerogel structure and also to the commencement of coordinative water elimination from the $[TbL_3(H_2O)_3]$ structure. The mass loss recorded in the second stage in 270–580 °C range can be attributed to the progressive poly-condensation and dehydration processes occurring in aerogel structure, and to the decomposition processes in the complex structure. Comparable results are reported in literature [20] where a mass loss of 14 % was recorded in the same temperature range, the slightly higher values recorded in case of the prepared photoluminescent aerogel can be attributed to the different amounts of organic phase trapped in the aerogel structure compared to reference results.

Experimental laboratory tests performed with a doped aerogel prepared in the conditions mentioned above show that it withstands successfully to the exposure at temperatures ranged between 100 and 200 °C for more than 1 h. Therefore, it shows an excellent preservation of the photoluminescent properties most probably due to the remarkable thermal insulation of the aerogel matrix that protects the embedded complex from thermal attack. In these conditions a thermal annealing procedure may be additionally possible after the critical point drying of the doped aerogel in order to eliminate the trapped water in the aerogel structure. However, the procedure should be performed preferably under vacuum at temperatures below 100 °C to avoid the loss of coordinated water within the structure of the $[TbL_3(H_2O)_3]$ complex.

Table 2 Results of the BET analysis for the unloaded aerogel sample

BET Surface (m^2/g)		342
Specific cumulative pores surface (m^2/g)	Adsorption	353
	Desorption	432
Medium pore diameter (nm)	Adsorption	115.8
	Desorption	97.7
Cumulative pores volume (cm^3/g)	Adsorption	1.02
	Desorption	1.05

3.4 BET Surface Area and pore size analysis

The BET investigation was performed only in case of undoped aerogel in order to evaluate its structure according to the chosen preparation path, since an alkaline catalyst usually leads to a prevalent meso-macroporous structure due to the dissolution-reprecipitation and Ostwald ripening processes which are favored [21]. Table 2 presents the results recorded for the undoped silica aerogel. The prepared aerogel includes all the three types of pores but as might be noted, the average pore diameter is approx. 100 nm which indicates a predominant macroporous structure, most probable due to the alkaline catalyst used in the gelation stage.

3.5 Scanning electron microscopy (SEM)

SEM images recorded for the photoluminescent aerogel support the conclusions provided by FT-IR, XRD and BET analyses and also the experimental observations regarding the low leaching of the complex during the solvent exchange operations requested by the aerogel preparation. Figure 4 presents SEM images recorded at 10 k (a) and 50 K magnification (b). Both images obtained show a typical structure for a generic silica aerogel prepared in analogue conditions [6]. The image obtained at 50 k magnification shows a solid phase composed of clusters with average sizes of 120–150 nm weakly connected into the aerogel skeletal network.

The macroporous structure with average pore size of 100–120 nm determined by nitrogen adsorption–desorption isotherms and BET analysis is also supported by the recorded SEM images. As can be noted, the distribution of macropores in the structure is not homogeneous, certain areas with a higher degree of aggregation being observed. This configuration suggests the presence of $[TbL_3(H_2O)_3]$ complex rather attached to the solid phase in aerogel structure than in macropores, fact which is due most likely to the interactions between chemical groups of complex with those specific to silica matrix. While the homogeneity and macroporous structure of a certain aerogel depends mainly on a series of parameters involved in the synthesis

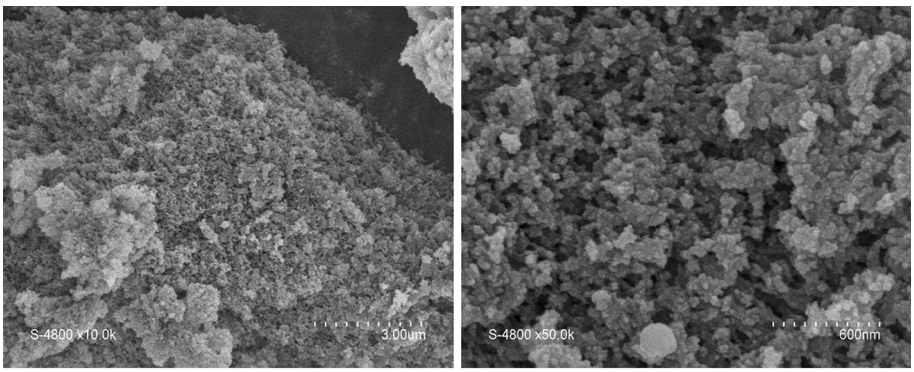

Fig. 4 SEM images recorded for the photoluminescent aerogel **a** 10 k resolution, **b** 50 k resolution

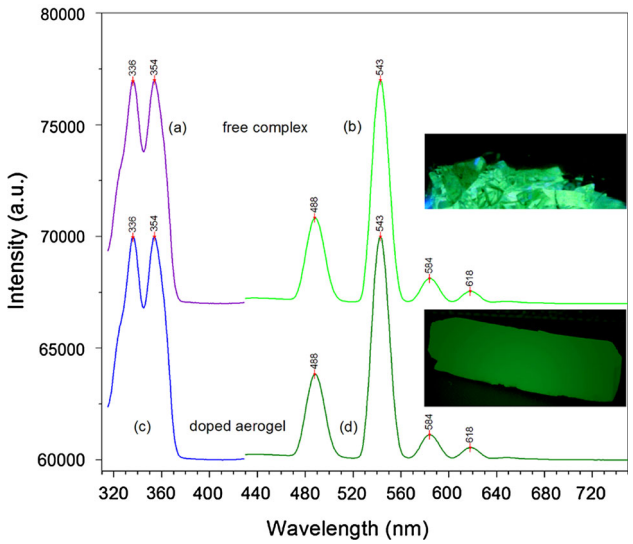

Fig. 5 Excitation and emission normalized spectra recorded for $[TbL_3(H_2O)_3]$ complex (*a*,*b*)/prepared photoluminescent aerogel (*c*,*d*)

path (such as silica precursor, solvent, type of catalyst, ageing and drying conditions) [6] similar experimental results were obtained for samples prepared under the same conditions. As already stated, the $[TbL_3(H_2O)_3]$ complex is attached to the aerogel framework so that the distribution of macropores seems to not have an important role in obtaining the overall properties of the prepared photoluminescent aerogel.

3.6 Fluorescence spectroscopy

The photoluminescence of the prepared aerogel is totally dependent on the properties of the embedded complex. The unique spectral properties of the trivalent lanthanide cations arise from the f—f transitions within 4f orbitals, which are partially shielded by the 5 s and 5p orbitals [22]. This leads to minimal interactions with the molecular entities located in the vicinity of the lanthanide cation. The inner shell electronic transitions are barely affected by a certain ligand or surroundings, thus, characteristic narrow emission bands and excited states lifetimes in millisecond range are achieved. Hence, the emission and excitation spectra recorded for the prepared aerogel are essentially the same as those recorded for the free complex. Its luminescence arises from the specific inner transitions of the Tb^{3+} cation [23, 24] within the surrounding crystalline field, no ligand centered luminescence being detected in the recorded emission spectra. Figure 5 presents excitation (a) and emission (b) spectra recorded for the free complex and also the excitation (c) and emission (d) spectra of the $[TbL_3(H_2O)_3]$ doped aerogel. In both cases, the emission spectra were recorded under the 354 nm excitation wavelength, while the excitation spectra were recorded by monitoring the 543 nm emission peak. The diagram-embedded pictures of both free complex (powder) and photoluminescent aerogel (40 × 10 × 10 mm monolith) were taken under excitation with a 4 W UV-A Philips TL4WBLB fluorescent lamp with a 360–370 nm peak emission.

Significant Tb^{3+} radiative emission peaks were recorded at 488, 543, 584 and 618 nm due to $^5D_4 \rightarrow {}^7F_6$, $^5D_4 \rightarrow {}^7F_5$, $^5D_4 \rightarrow {}^7F_4$ and $^5D_4 \rightarrow {}^7F_2$ radiative transitions [23, 25]. The lower intensity 584 nm peak due to $^5D_4 \rightarrow {}^7F_5$ transition is known to be moderately affected by the surroundings symmetry. The two intense emission bands centered at 488 and 543 nm are practically unaffected by the symmetry of the crystalline field surroundings [26]. The excitation spectra recorded (Fig. 5a, c) present two peaks centered at 336 and 354 nm.

The influence of the silica matrix over the photoluminescent properties of the complex is negligible, similar spectra being recorded for the prepared aerogel (Fig. 5d). Likewise, the ratio between intensity of the recorded peaks is virtually identical with the case of free complex. The relative intensity of the photoluminescent emission of the aerogel embedded complex was compared with the free complex emission intensity prior to embedding while keeping the same measurement parameters (excitation and

emission slits, angle of the powder adapter turret etc.). The excitation peaks recorded for the aerogel are centered at exactly the same wavelengths as recorded for the free complex. The only noticeable difference, which was also visually observed, is the lower overall emission intensity. This situation is most probably due to the lower penetration of the excitation radiation in the aerogel volume to reach the embedded $[TbL_3(H_2O)_3]$ complex. The distribution homogeneity of the macropores in the aerogel matrix and the pore size distribution play a negligible role in achieving the overall photoluminescent properties of the doped aerogels since the $[TbL_3(H_2O)_3]$ complex, which is responsible for these properties is rather attached to the solid phase in aerogel structure than in macropores.

Despite of a slightly lower photoluminescence of the doped aerogel compared with the free complex, the embedment in the aerogel structure offers a series of advantages such as long term preservation of properties due to the decoupling of the complex structure from ambient conditions (the free complex is moisture sensitive) [12]; thermal stability is greatly improved especially in the temperature range where most of the potential applications would require. Another advantage consists in the possibility to obtain a photoluminescent material with various shapes by simply using the desired shaped-recipient during gelation stages of the preparation process.

4 Conclusion

The paper reports the preparation of a photoluminescent silica aerogel through embedding in a silica matrix of a new prepared Tb(III) complex using NHSI as ligand. The remarkable photoluminescence of the free complex as a result of specific radiative transitions within the Tb(III) cation with the most intense peak located at 543 nm due to $^5D_4 \rightarrow {}^7F_5$ transition are preserved by the prepared aerogel. Both, free complex and doped aerogel were investigated through thermal analysis, FT-IR, powder X-ray diffraction, SEM and fluorescence spectroscopy. The leaching of the free complex in the solvent medium used in various stages required by the aerogel preparation was found to be minimal due to the interactions occurring between the functional groups of the $[TbL_3(H_2O)_3]$ complex and silica matrix. This conclusion was also supported by both experimental observations, and data obtained through the above mentioned investigation techniques. The remarkable photoluminescent emission of the prepared aerogel and also the excitation spectra, conveniently located in the UV-A region, may recommend it for applications in optoelectronics.

Acknowledgments This work was supported by a grant of the Romanian National Authority for Scientific Research, CNCS–UEFISCDI, Project Number PN-II-ID-PCE-2011-3-0708.

References

1. Gurav JL, Jung IK, Park HH, Kang ES, Nadargi DY (2010) J Nanomater 2010:1–11
2. Shewale PM, Rao AV, Rao AP, Bhagat SD (2009) J Sol–Gel Sci Technol 49:285–292
3. Collinson MM (1998) Mikrochim Acta 129:149–165
4. Glauser SAC, Lee HWH (1997) MRS Proc 471:331–334
5. Lorenz C, Emmerling A, Fricke J, Schmidt T, Hilgendor M, Spanhel L, Muller G (1998) J Non-Cryst Solids 238:1–5
6. Aegerter MA, Leventis N, Koebel M (2011) Aerogels handbook. Springer, New York
7. Sorensen L, Strouse GF, Stiegman AE (2006) Adv Mater 18:1965–1967
8. Binnemans K (2009) Chem Rev 109:4283–4347
9. Jin T, Tsutsumi S, Deguchi Y, Machida K, Adachi G (1997) J Alloys Compd 252:59–66
10. Jin T, Inoue S, Machida K, Adachi G (1998) J Alloys Compd 265:234–239
11. Godlewska P, Macalik L, Hanuza J (2008) J Alloys Compd 451:236–239
12. Stan CS, Rosca I, Sutiman D, Secula MS (2012) J Rare Earth 30:401–407
13. Soleimani DA, Abbasi MH (2008) J Mater Proc Technol 199:10–26
14. Suh DJ, Park TJ, Sonn JH, Lim JC (1999) J Mater Sci Lett 18:1473–1475
15. Pierre AC, Pajonk GM (2002) Chem Rev 102:4243–4246
16. Premkumar T, Govindarajan S, Rath NP, Manivannan V (2009) Inorg Chim Acta 362:2941–2946
17. Kim EJ, Kim CH, Kim JK, Yun SS (2008) Bull Korean Chem Soc 29:1157–1161
18. Music S, Filipovic-Vincekovic N, Sekovanic L (2011) Braz J Chem Eng 28:89–94
19. Mane AU, Greene JP, Nolen JA, Sampathkumaran U, Owen TW, Winter R, Elam JW (2012) Appl Surf Sci 258:6472–6478
20. Folgar C, Folz D, Suchicital C, Clark D (2007) J Non-Cryst Solids 353:1483–1490
21. Zeng HC (2007) Curr Nanosci 3:177–181
22. Cotton SA (2006) Lanthanide and actinide chemistry. Ed.Wiley & Sons, Chicester
23. Liu G, Jacquier B (2005) Spectroscopic properties of rare earth in optical materials. Springer, Berlin
24. Bunzli JCG, Piguet C (2005) Chem Soc Rev 34:1048–1077
25. Kottas GS, Mehlstubl M, Fröhlich R, De Cola L (2007) Eur J Inorg Chem 2007:3465–3468
26. Kang JG, Kim TJ (2005) Bull Korean Chem Soc 26:1057–1064